

3. DATA REPORT: GEOCHEMICAL ANALYSES OF HYDROTHERMALLY ALTERED SEDIMENTS FROM THE CONVERGENT COSTA RICAN MARGIN¹

Valerie Chavagnac,² Laura Font,^{2,3} J. Andy Milton,²
and Ian W. Croudace²

ABSTRACT

Bulk geochemical analyses were carried out on 27 sediment samples located just above the igneous section of the incoming plate along the Costa Rican convergent margin. This pilot study was intended to determine whether hydrothermal activity within the sediment section could be detected within the bulk sediment. The metaliferous index ($100 \times \text{Al}/[\text{Al} + \text{Fe} + \text{Mn}]$) values on bulk sediment ($24.3 < x < 43.3$) are all much lower than the value for deep pelagic sediment (50.8) but higher than the value for the hydrothermal sulfide from the East Pacific Rise (1). The high Zn, Cu, and Co concentrations associated with high Ba content for a constant detrital input (molar $\text{Ti}/\text{Al} = 0.121 \pm 0.026$) indicate that the transition metal enrichment is not related to volcanic ash but rather to Fe-Mn oxides, sulfides, and barite. These observations testify to a record of hydrothermal activity within the 70 m of sediment overlying the basement.

INTRODUCTION

At the Costa Rican convergent margin, coring during Ocean Drilling Program (ODP) Legs 170 and 205 and associated postcruise studies identified the occurrence of three hydrological systems, one of which is acting within the uppermost part of the incoming oceanic crust. The

¹Chavagnac, V., Font, L., Milton, J.A., and Croudace, I.W., 2006. Data report: Geochemical analyses of hydrothermally altered sediments from the convergent Costa Rican margin. In Morris, J.D., Villinger, H.W., and Klaus, A. (Eds.), *Proc. ODP, Sci. Results*, 205, 1–16 [Online]. Available from World Wide Web: <http://www-odp.tamu.edu/publications/205_SR/VOLUME/CHAPTERS/207.PDF>. [Cited YYYY-MM-DD]

²National Oceanography Centre, Waterfront Campus, European Way, Southampton SO14 3ZH, United Kingdom. Correspondence author: vmcc@noc.soton.ac.uk

³Department of Earth Sciences, University of Durham, Durham DH1 3LE, United Kingdom.

existence of active fluid flow is substantiated by particularly low heat flow and by the pore fluid chemistry of basal sediments, which show similar characteristics to modern seawater (Kimura, Silver, Blum, et al., 1997). Sediment samples were collected from the sediment section of Subunit U3C overlying the incoming igneous section during Leg 205 on the Costa Rica convergent margin. This study was undertaken to determine whether low-temperature hydrothermal activity is recorded by sediment and to identify the geochemical features of low-temperature hydrothermal activity.

Leg 205 Site 1253 is located ~1 km away from Leg 170 Site 1039 and ~200 m seaward of the deformation front in the deepest part of the Middle America Trench (Morris, Villinger, Klaus, et al., 2003). Three sedimentary units and one gabbro sill were recognized at Site 1039. Unit U1 is composed of dark green diatomaceous ooze with ash layers and is underlain by Unit U2, which contains essentially clays. Basal Unit U3, which is divided into Subunits U3A, U3B, and U3C, exhibits a dramatic increase in biogenic sedimentation (nannofossil ooze) with minor ash layers. Sediment coring began at Site 1253 at 370 meters below seafloor (mbsf), within Subunit U3C. A mixture of nannofossil chalks with varying subordinate proportions of clay dominates the 70 m of recovered sediments (370–440 mbsf). A gabbro sill, Subunit U4A, intrudes the sediment Subunit U3C between 400 and 430 mbsf. The igneous intrusion modified the structure of the upper 3 m above it by driving strong diagenesis, lithification, and lamination. Below the gabbro sill, less lithified nannofossil chalks were recovered, but they are identified as the same lithologic unit as above the sill. We will refer in this study to sediment samples from Subunit U3C located below and above Subunit U4A but all located above Subunit U4B (i.e., the lower igneous unit). The dominant sediment is biogenic carbonate with <5% dark green clay layers. The sediment section has preserved a lamination fabric acquired during deposition under the influence of current activity. In addition, volcanic ash layers are an important minor lithology but do not represent more than 1% of the total stratigraphy. Sediment with the lowest proportion of detrital input exhibits a light color, so we collected a suite of samples at regular intervals showing the lowest proportion of dark green clay. Based on paleomagnetic analyses and biostratigraphy, the sediment section overlying the igneous section sampled for this study is between 15.6 and 18.21 Ma (Morris, Villinger, Klaus, et al., 2003; A. Strasser, pers. comm., 2004). Sediments sampled here are distinct from the basal carbonates at Leg 170 Site 1039, which show pronounced lie-segang structures and other visual indicators of hydrothermal activity (Kimura, Silver, Blum, et al., 1997).

We present chemical analyses for major elements and carbonate contents along with trace element concentrations (transition metals and large ion lithophiles) for 27 sediment samples. Fourteen samples were selected above the igneous Subunit U4A between 370 and 400 mbsf (Cores 205-1253A-1R through 5R) and thirteen samples below at a depth interval of 430–440 mbsf (Cores 205-1253A-10R through 11R).

ANALYTICAL METHODS

Major and trace element concentrations of 27 sediment samples are reported in Table T1.

The CaCO₃ content was determined by coulometric titration with a UIC model 5012 CO₂ coulometer at National Oceanography Centre,

Southampton (NOCS) (United Kingdom). Percent content was determined from CO₂ liberated by 10% phosphoric acid, using 25–30 mg of sample. Calibration of the instrument was performed using a pure CaCO₃ standard. Reference standard sediment 10549#1K (pure CaCO₃) was run every ~6 samples to check the calibration of the instrument, followed by a blank.

Sediment samples were dried for 24 hr in an oven at 50°C before grinding to a fine powder in an agate mortar to minimize metal contamination. For bulk-rock analyses of major element oxides, 0.8000 g of the dried powdered sample was prepared by fusing with 4.0000 g of a lithium tetraborate flux (Li₂B₄O₇) at 1150°C in a furnace followed by casting into a Pt-Au dish. The 31-mm-diameter glass beads were then analyzed using a Panalytical Magix-Pro wavelength dispersive X-ray fluorescence spectrometer at NOCS. The total measurement time was ~15 min, but the time spent on each element peak and background position depended on the element. Major element calibrations were based on measurements of >15 international geochemical reference materials (GRMs). Interelement coefficients were determined using SuperQ 4 XRFA software (Panalytical) that employed fundamental parameter algorithms. Analytical precision was generally better than 1% (relative standard deviation [rsd]), whereas accuracy was typically within 5% of the consensus or working values of good-quality GRMs. Marine sediment USGS MAG-1 (marine mud) and calcareous marine mud (GeoPT CH-1) were analyzed to assess accuracy and compared favorably with the working values (within 5% rsd). The methods used are adaptations of those reported by Croudace and Williams-Thorpe (1988). Loss on ignition was determined by igniting a 1-g sample at 950°C for 4 hr and measuring the weight loss.

For trace element analysis, ~200 mg of powdered sample was weighed in a 17-mL polytetrafluoroethylene (PTFE) beaker and was dissolved in the sealed beaker on a hotplate (~130°C) using a 3:1 mixture of concentrated HF and HNO₃. After 3 days on a hotplate, the solution was then dried and converted to chlorides by adding 10 mL of 6-M HCl. A blank solution was treated in the same manner as the sample and represents a total chemistry blank solution. The reagents used in the dissolution procedures are all high purity, double-subboiled distilled acids. Hence, the blank solution for all elements considered here are <1% of the analyte. Following complete dissolution, a weighed aliquot of that solution was evaporated to dryness and redissolved in 2% HNO₃ (spiked with 10 ppb In and Re for internal correction). A dilution factor of 2000–4500 was applied to each sample and rock standard. This solution was analyzed for metal and large-ion lithophile elements by inductively coupled plasma–mass spectrometry (VG Plasmaquad PQ2+) at NOCS. The instrument was calibrated using four international rock standards, JB-2, JB-1A, JB-3, and BRR-1, which were run before, during, and after each group of analyses. The data processing procedure includes linear drift correction, interference corrections, blank subtraction, calibration with international standards, and a dilution correction. Additional high-Ba concentration synthetic standards were made for Ba measurements. In-run precision was routinely in the 1%–5% range, with Cs and Zn in JB-1A being worse than 10%. Measured and reference values for JB-2 and JB-1A are shown in Table T2 to demonstrate the accuracy of the analysis.

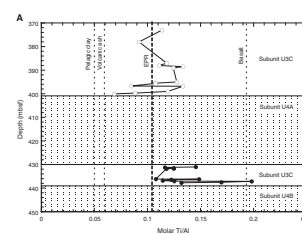
RESULTS

Petrographic observation of the sediment samples by smear slides indicates the contribution of four different components during the Miocene in the North Pacific: biogenic carbonate, volcanic ash, detrital clay, and biogenic silica. These four distinct components are typical of North Pacific sediments (Kyte et al., 1993). Ti and Al values were used to evaluate the detrital component of the sediments (Fig. F1). Values of the molar Ti/Al ratio from Subunit U3C sediments (0.121 ± 0.026) are significantly higher than those typical of pelagic clay (molar Ti/Al = 0.057) (Kyte et al., 1993) and volcanic ash (molar Ti/Al = 0.05) (Clift et al., 2005) but similar to metaliferous sediments from the East Pacific Rise (molar Ti/Al = 0.11) (Schaller et al., 2000). There is no linear relationship of Ti/Al with Fe_2O_3 , suggesting that the detrital sources remained unchanged both in terms of source and proportion during the Miocene. These two observations argue that at this location during the Miocene, Ti and Al values reflect two different sources, an aeolian source together with a local source with Ti/Al values higher than volcanic ash.

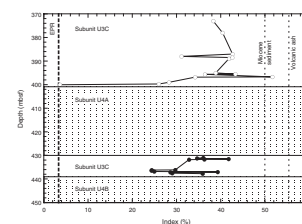
Böstrom et al. (1969) proposed use of the index $100 \times \text{Al}/(\text{Al} + \text{Fe} + \text{Mn})$, to discriminate between metaliferous and nonmetaliferous pelagic sediments. Figure F2 shows a depth profile between 370 and 450 mbsf of the index value. Pelagic sediments composed of a mixture of biogenic and detrital material have an index value >50 , such as 60.8 measured for the present-day deep-sea Pacific clay, with values of 50.8 during the Miocene (Kyte et al., 1993). Metalliferous sediments such as those along the East Pacific Rise and Juan de Fuca Ridge exhibit index values much lower than 50 and as low as 1 (German, et al., 1997, 1999). The index values for the majority of the sediment suite collected at Site 1253 vary between 24.3 and 43.3, with two extreme cases at 3.6 and 51.6. The lower values suggest a significant hydrothermal component in much of the Miocene basal sediment.

Transition metal concentrations such as Cu, Co, Zn, Fe, V, and Ti remain high in the sediment just above the igneous section Subunit U4B and at several intervals within the 70 m of Subunit U3C, reaching levels that are ~2–3 times those seen in the overlying carbonate Subunit U3A (Table T2). Ba also exhibits very high concentrations in these strata. The positive linear relationship between Co and Cu with Ba is generally not seen in siliceous arc volcanic rocks, suggesting that the element enrichment is not a characteristic of the volcanic ash (Fig. F3). Rather, the occurrence of phases like Fe-Mn oxides, sulfides, and barite is more dominant in sediment sections with little biogenic contribution. Previous geochemical studies of sediment from ODP Legs 138 and 170 as well as those from Deep Sea Drilling Project Leg 67 Site 495 identified (visually and chemically) 2.5 to 30 m of basal metaliferous sediment above basement (Mayer, Pisias, Janecek, et al., 1992; Shipboard Scientific Party, 1982; Kimura, Silver, Blum, et al., 1997). Here, the metal enrichments are thought to derive from hydrothermal activity most likely related to a high-temperature hydrothermal system along the ridge axis, overprinted by a low-temperature hydrological system within the upper oceanic crust, similar to those observed along the flank of the Juan de Fuca Ridge (Fisher and Davis, 2000).

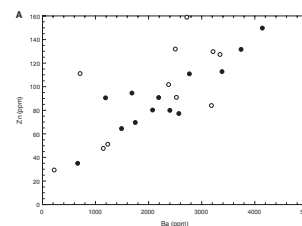
F1. Ti/Al vs. depth, CaO_3 , and Fe_2O_3 , p. 7.



F2. Metaliferous sediment index values, p. 10.



F3. Zn, Cu, and Co vs. Ba, p. 11.



ACKNOWLEDGMENTS

This research used samples and/or data provided by the Ocean Drilling Program (ODP). ODP is sponsored by the U.S. National Science Foundation (NSF) and participating countries under management of Joint Oceanographic Institutions (JOI), Inc. V. Chavagnac is funded by the 2000 Southampton Oceanography Centre Research Fellowship. Hydrothermal studies at NOCS are supported by the Natural Environment Research Council core strategic program.

REFERENCES

- Boström, K., Peterson, M.N.A., Joensuu, O., and Fisher, D.E., 1969. Aluminum-poor ferromanganoan sediments on active oceanic ridges. *J. Geophys. Res.*, 74:3261–3270.
- Clift, P. D., L. Chan, J. Blusztajn, G. D. Layne, M. Kastner, and R. K. Kelly (2005), Pulsed subduction accretion and tectonic erosion reconstructed since 2.5 Ma from the tephra record offshore Costa Rica, *Geochem. Geophys. Geosys.*, 6:Q09016. [doi:10.1029/2005GC000963](https://doi.org/10.1029/2005GC000963)
- Croudace, I.W., and Williams Thorpe, O., 1988. A low dilution, wavelength dispersive X-ray fluorescence procedure for the analysis of archaeological rock artefacts. *Archaeometry*, 30:227–236.
- Fisher, A.T., and Davis, E.E., 2000. An introduction to the scientific results of Leg 168. In Fisher, A.T., Davis, E.E., and Escutia, C. (Eds.), *Proc. ODP, Sci. Results*, 168: College Station TX (Ocean Drilling Program), 3–5. [[HTML](#)]
- German, C.R., Bourles, D.L., Brown, E.T., Hergt, J., Colley, S., Higgs, N.C., Ludford, E.M., Nelsen, T.A., Feely, R.A., Raisbeck, G., and Yiou, F., 1997. Hydrothermal scavenging on the Juan de Fuca Ridge: $^{230}\text{Th}_{\text{xs}}$, ^{10}Be , and REEs in ridge-flank sediments. *Geochim. Cosmochim. Acta*, 61:4067–4078. [doi:10.1016/S0016-7037\(97\)00230-5](https://doi.org/10.1016/S0016-7037(97)00230-5)
- German, C.R., Hergt, J., Palmer, M.R., and Edmond, J.M., 1999. Geochemistry of a hydrothermal sediment core from the OBS vent-field, 21°N East Pacific Rise. *Chem. Geol.*, 155:65–75. [doi:10.1016/S0009-2541\(98\)00141-7](https://doi.org/10.1016/S0009-2541(98)00141-7)
- Kimura, G., Silver, E.A., Blum, P., et al., 1997. *Proc. ODP, Init. Repts.*, 170: College Station, TX (Ocean Drilling Program). [[HTML](#)]
- Kyte, F.T., Leinen, M., Heath, G.R., and Zhou, L., 1993. Cenozoic sedimentation history of the central North Pacific: inferences from the elemental geochemistry of Core LL44-GPC3. *Geochim. Cosmochim. Acta*, 57:1719–1740. [doi:10.1016/0016-7037\(93\)90109-A](https://doi.org/10.1016/0016-7037(93)90109-A)
- Mayer, L., Pisias, N., Janecek, T., et al., 1992. *Proc. ODP, Init. Repts.*, 138 (Pts. 1 and 2): College Station, TX (Ocean Drilling Program).
- Morris, J.D., Villinger, H.W., Klaus, A., et al., 2003. *Proc. ODP, Init. Repts.*, 205 [CD-ROM]. Available from: Ocean Drilling Program, Texas A&M University, College Station TX 77845-9547, USA. [[HTML](#)]
- Schaller, T., Morford, J., Emerson, S.R., and Feely, R.A., 2000. Oxyanions in metalliferous sediments: tracers for paleoseawater metal concentrations? *Geochim. Cosmochim. Acta*, 63:2243–2254. [doi:10.1016/S0016-7037\(99\)00443-3](https://doi.org/10.1016/S0016-7037(99)00443-3)
- Shipboard Scientific Party, 1982. Site 495: Cocos plate–Middle America Trench outer slope. In Aubouin, J., von Huene, R., et al., *Init. Repts DSDP 67*: Washington (U.S. Govt. printing Office), 79–141.
- Turekian, K.K., and Wedepohl, K.H., 1961. Distribution of the elements in some major units of the Earth's crust. *Geol. Soc. Am. Bull.*, 72:175–192.

Figure F1. A. Depth profile of molar Ti/Al values. Molar Ti/Al value of pelagic clay (Kyte et al., 1993), volcanic ash (Clift et al., 2005) and basalt (Turekian and Wedepohl, 1961) are also reported for comparison along with values for East Pacific Rise (EPR) metaliferous sediment (Schaller et al., 2000). (Continued on next two pages.)

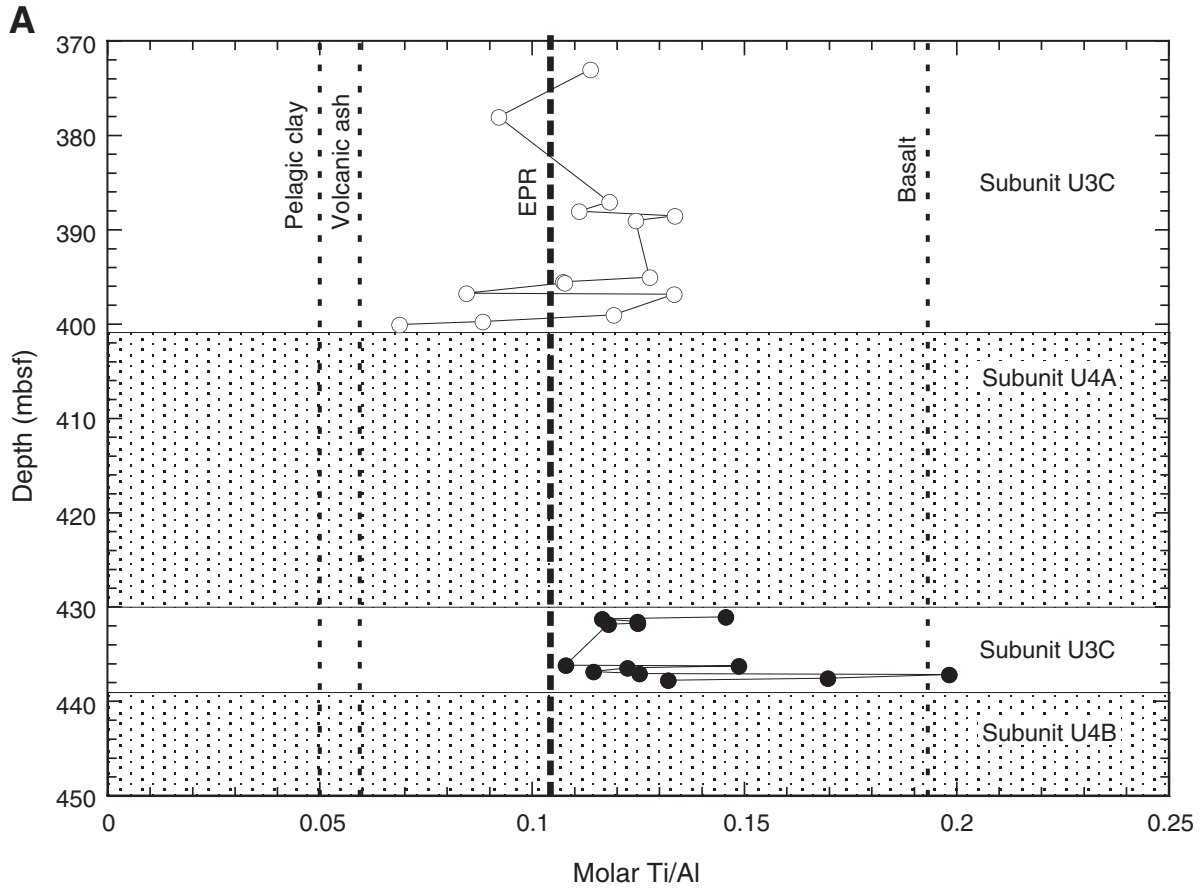


Figure F1 (continued). B. Molar Ti/Al value vs. CaCO_3 content. Solid circles = sediment samples just above Subunit U4B, open circle = sediment sample above Subunit U4A.

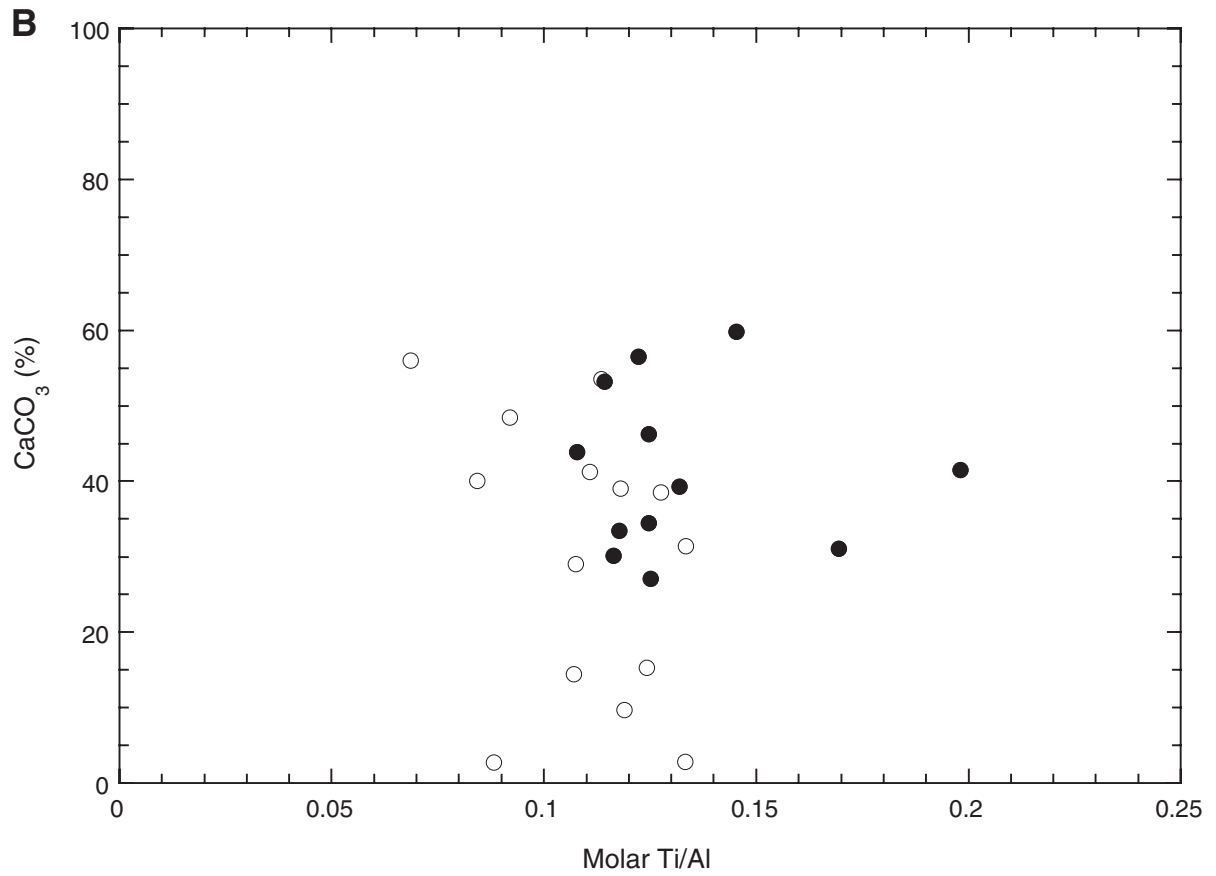


Figure F1 (continued). C. Molar Ti/Al value vs. Fe_2O_3 content. Solid circles = sediment samples just above Subunit U4B, open circles = sediment samples above Subunit U4A.

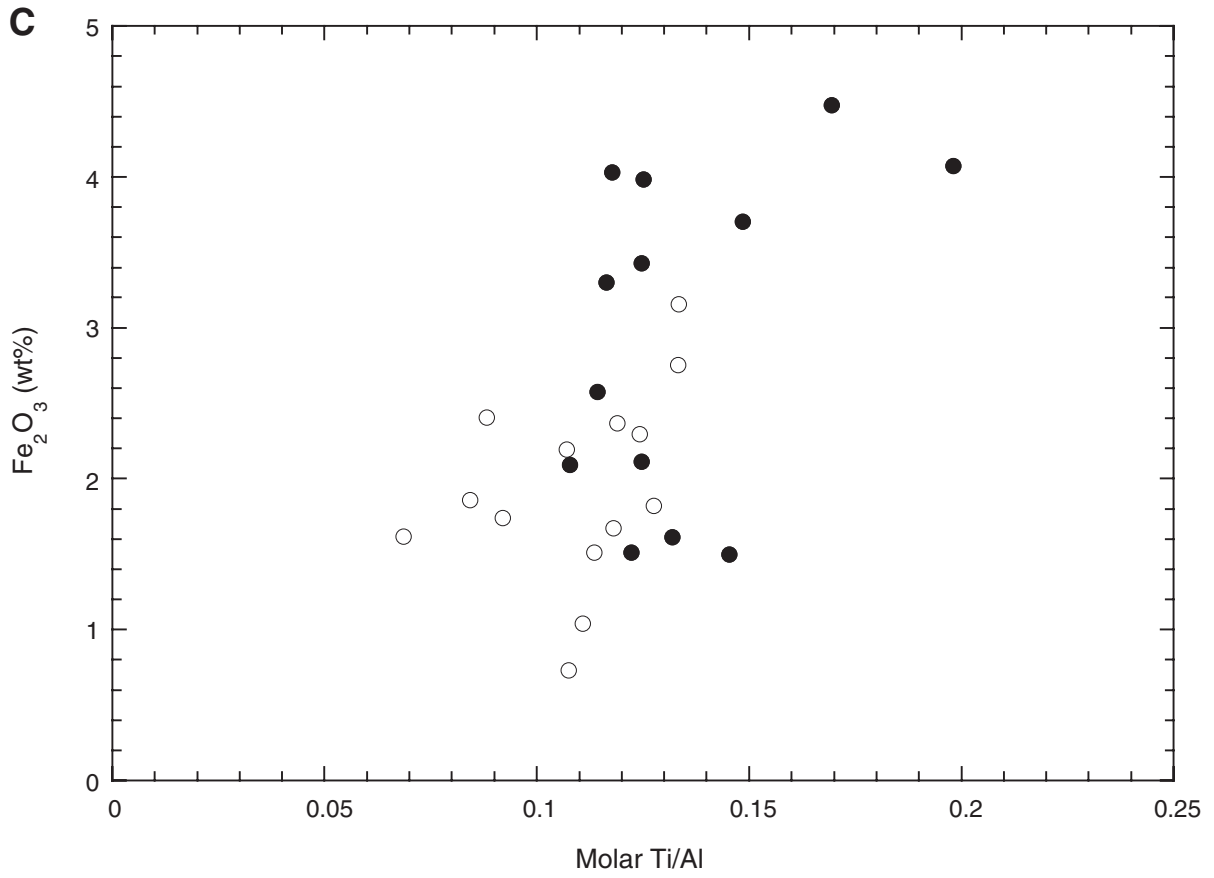


Figure F2. Depth profile of metaliferous sediment index percent values ($100 \times \text{Al}/[\text{Al} + \text{Fe} + \text{Mn}]$). Solid circles = sediment samples just above Subunit U4B, open circles = sediment samples above Subunit U4A. Average index value of metaliferous sediments found along the East Pacific Rise (EPR) (Schaller et al., 2000) and in Miocene sediment (Kyte et al., 1993) and volcanic ash (Clift et al., 2005) are also reported for comparison.

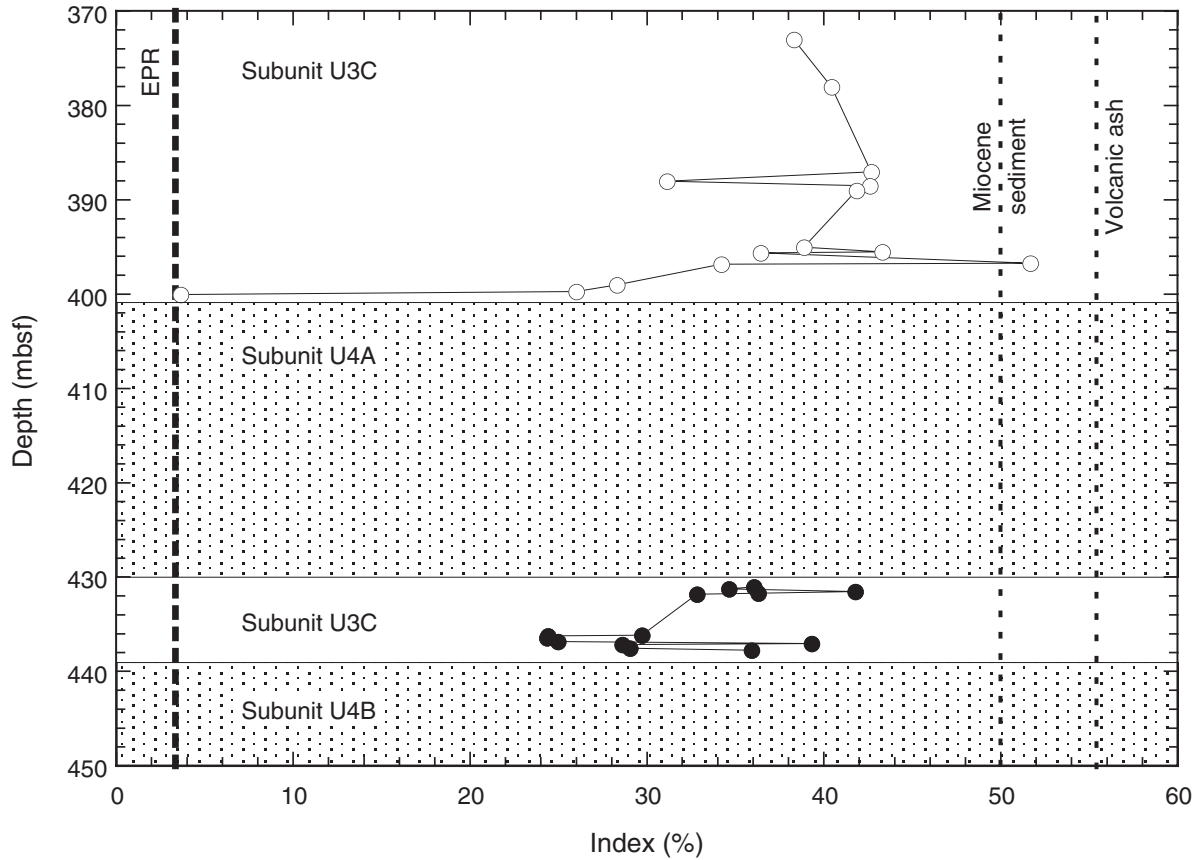


Figure F3. Elemental content as a function of Ba content. Solid circles = sediment samples just above Subunit U4B, open circles = sediment samples above Subunit U4A. A. Zn. (Continued on next two pages.)

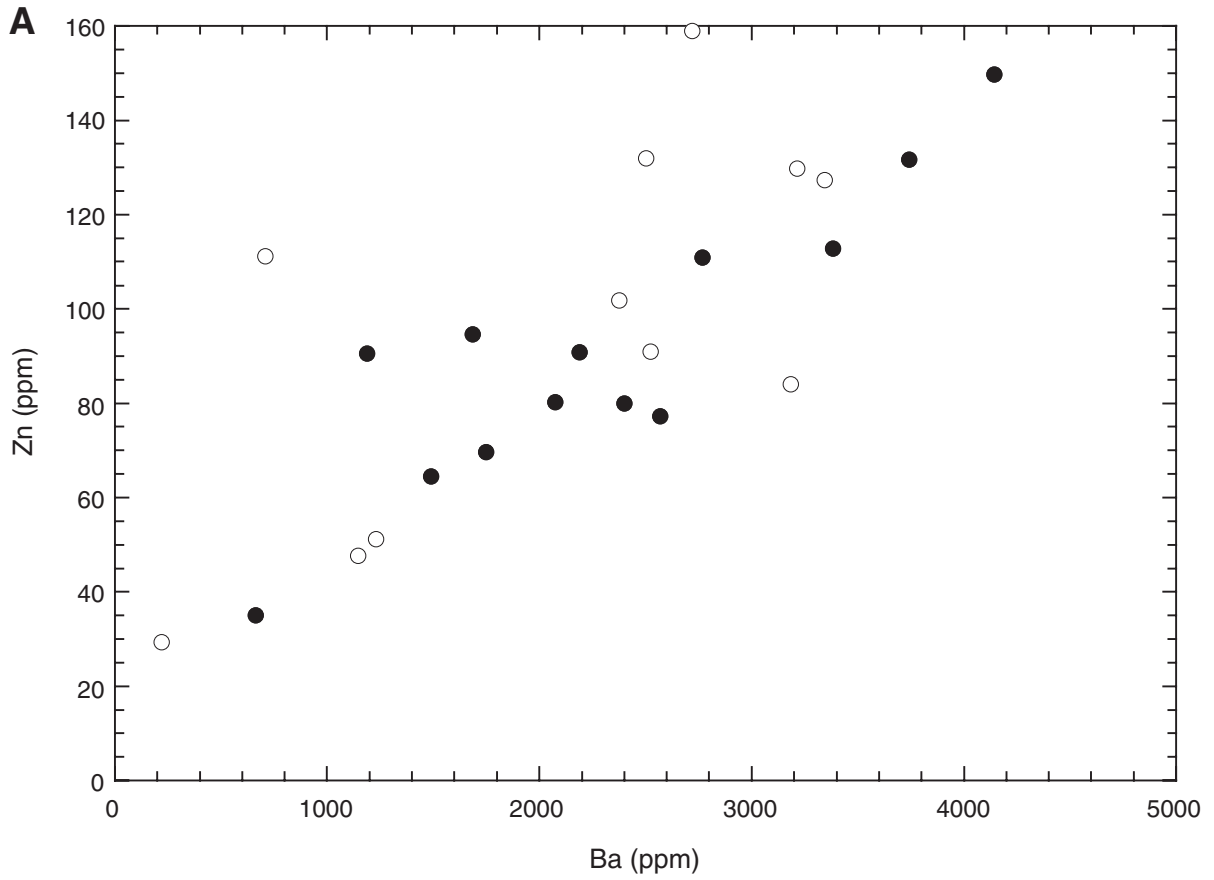


Figure F3 (continued). B. Cu.

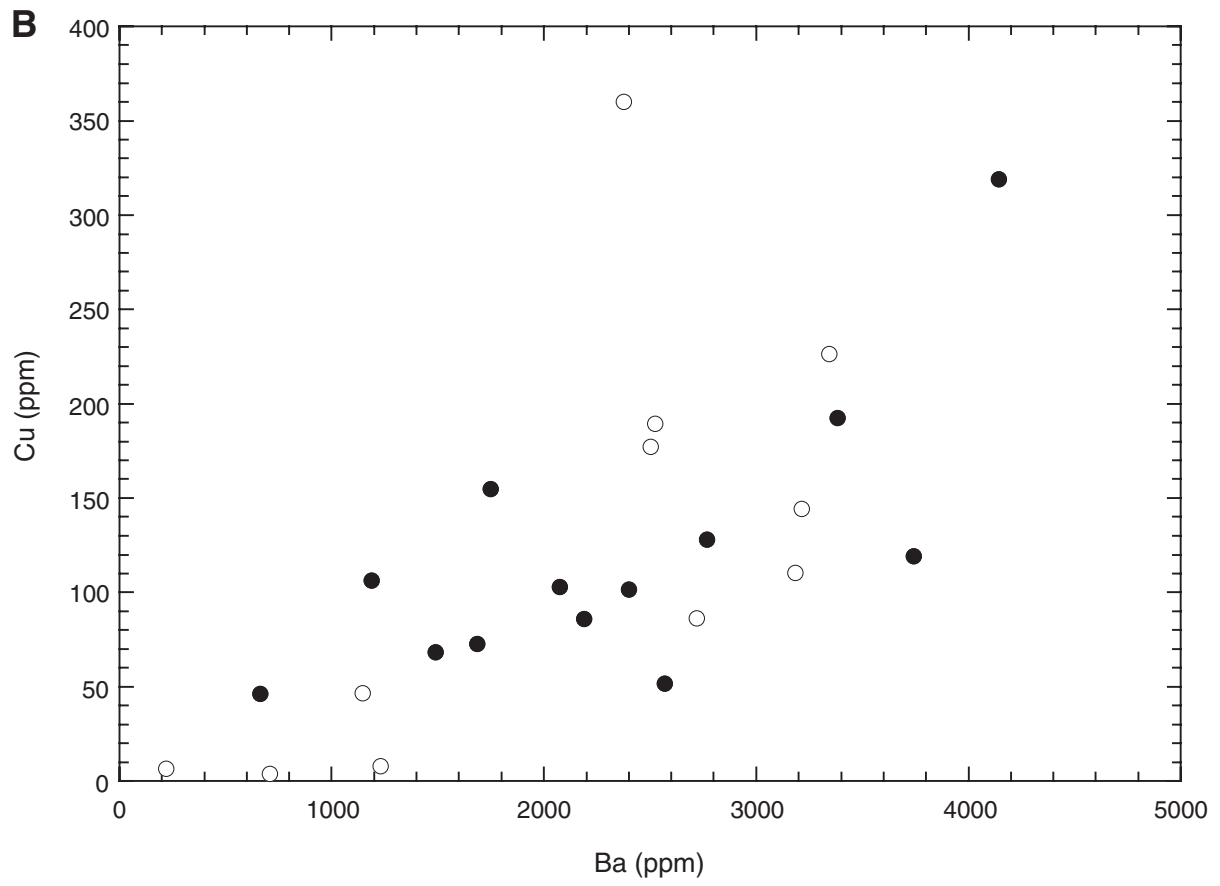


Figure F3 (continued). C. Co.

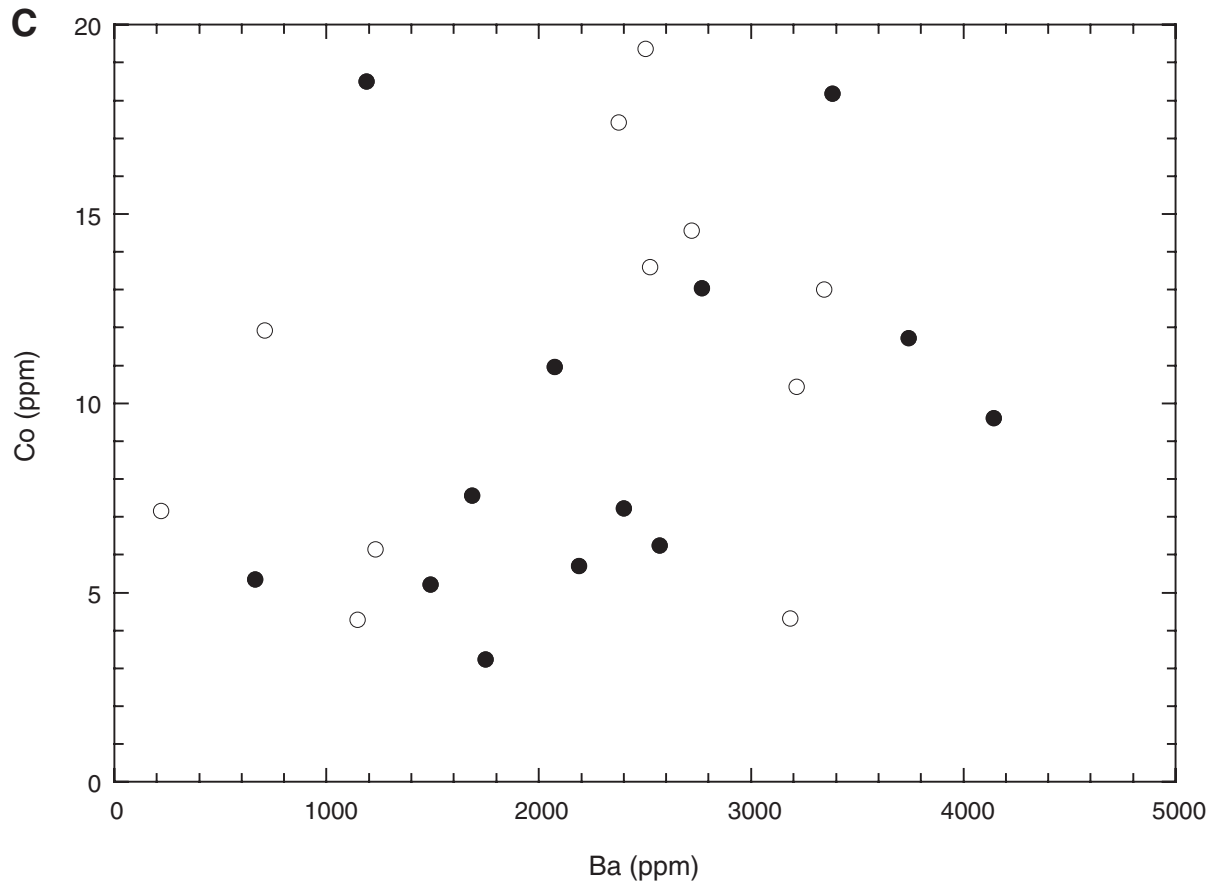


Table T1. Major and trace element composition of sediment samples from Subunit U3C, Site 1253. (Continued on next page.)

Core, section, interval (cm)	Depth (mbsf)	Major element oxide (wt%)											LOI (%)	CaCO ₃ (%)	Ti/Al (molar)	Index (%)
		SiO ₂	TiO ₂	Al ₂ O ₃	Fe ₂ O ₃	MnO	MgO	CaO	K ₂ O	Na ₂ O	P ₂ O ₅	Total				
205-1253A-*																
1R-2, 31-33	373	28.68	0.13	1.46	1.51	0.24	0.64	37.93	0.32	1.72	0.09	72.73	33.19	53.58	0.114	38.3
2R-2, 28-30	378	32.77	0.13	1.83	1.74	0.28	0.68	35.24	0.52	2.13	0.09	75.41	30.10	48.41	0.092	40.4
3R-2, 3-5	387	35.31	0.17	1.89	1.67	0.23	0.71	34.23	0.41	1.94	0.12	76.68	28.67	39.04	0.118	42.7
3R-2, 92-94	388	44.49	0.06	0.77	1.04	0.23	0.50	29.40	0.26	1.96	0.07	78.78	25.81	41.25	0.111	31.1
3R-3, 13-16	388.5	44.19	0.33	3.25	3.15	0.15	1.34	24.09	0.47	2.18	0.08	79.23	24.53	31.36	0.133	42.6
3R-3, 77-79	389	51.99	0.23	2.44	2.29	0.25	2.08	22.05	0.37	1.61	0.12	83.44	20.00	15.28	0.124	41.8
4R-1, 15-16	395	46.37	0.17	1.81	1.82	0.30	1.22	25.68	0.32	1.61	0.07	79.37	24.64	38.51	0.128	38.8
4R-1, 37-39	395.5	62.55	0.19	2.36	2.20	0.13	1.73	12.51	0.32	1.87	0.04	83.89	18.06	14.45	0.107	43.3
4R-1, 43-44	395.6	55.22	0.06	0.75	0.73	0.23	0.80	22.59	0.18	1.30	0.06	81.92	21.61	29.04	0.108	36.4
4R-1, 66-67	396.7	41.93	0.20	3.15	1.86	0.34	1.45	26.38	0.61	1.70	0.09	77.70	26.41	40.08	0.084	51.6
4R-1, 79-81	396.8	70.71	0.21	2.11	2.75	0.29	5.84	6.98	0.09	1.36	0.07	90.42	10.67	2.83	0.133	34.2
4R-3, 79-80	399	57.59	0.12	1.32	2.37	0.16	17.83	2.75	0.15	1.77	0.07	84.12	16.31	9.69	0.119	28.3
4R-4, 44-46	399.7	63.36	0.08	1.25	2.40	0.27	20.04	3.73	0.18	1.86	0.09	93.26	7.32	2.71	0.088	26.0
5R-1, 0-5	400	11.80	0.11	2.14	1.62	37.59	4.48	11.59	0.28	0.52	0.21	70.34	31.47	55.97	0.069	3.6
205-1253A-†																
10R-2, 49-51	431.00	32.17	0.16	1.45	1.50	0.41	0.72	33.92	0.13	0.90	0.08	71.44	28.56	59.80	0.145	36.0
10R-2, 59-73	431.20	48.94	0.22	2.55	3.30	0.31	2.12	20.14	0.30	1.26	0.13	79.26	20.74	30.16	0.116	34.6
10R-2, 96-78	431.50	47.18	0.33	3.48	3.43	0.22	1.78	20.49	0.72	1.81	0.08	79.52	20.48	34.50	0.125	41.8
10R-2, 116-118	431.70	38.04	0.17	1.80	2.11	0.25	1.63	26.03	0.31	1.63	0.07	72.05	27.95	46.27	0.125	36.3
10R-2, 123-124	431.80	47.85	0.25	2.76	4.03	0.23	3.36	19.02	0.46	1.94	0.11	79.99	20.01	33.42	0.118	32.8
11R-1, 7-9	436.10	39.78	0.11	1.33	2.09	0.26	2.86	24.47	0.14	1.66	0.08	72.77	27.23	43.90	0.108	29.7
11R-1, 19-21	436.20	32.64	0.19	1.71	3.71	0.28	4.48	25.91	0.15	1.96	0.10	71.13	28.87	ND	0.149	24.4
11R-1, 38-40	436.40	31.75	0.08	0.83	1.51	0.39	2.13	31.86	0.17	1.47	0.09	70.28	29.72	56.46	0.122	24.3
11R-1, 81-96	436.80	24.28	0.11	1.28	2.58	0.31	3.51	28.33	0.11	0.85	0.10	61.46	38.54	53.18	0.114	24.9
11R-2, 2-4	437.00	50.31	0.34	3.60	3.98	0.21	3.90	18.24	0.35	2.11	0.08	83.11	16.89	27.11	0.125	39.3
11R-2, 14-16	437.10	38.03	0.35	2.33	4.07	0.30	4.84	24.91	0.19	1.67	0.09	76.76	23.24	41.46	0.198	28.6
11R-2, 34-35	437.50	42.32	0.33	2.54	4.47	0.21	4.71	17.41	0.20	2.20	0.10	74.49	25.51	31.02	0.169	29.0
11R-2, 54-56	437.70	48.18	0.14	1.39	1.61	0.24	1.31	21.81	0.27	1.41	0.09	76.43	23.57	39.23	0.132	35.9

Notes: LOI = loss on ignition. ND = not determined. * = above Subunit U4A, † = above Subunit U4B and below Subunit U4A.

Table T1 (continued).

Core, section, interval (cm)	Depth (mbsf)	Trace elements (ppm)											
		Sc	Rb	Sr	Y	Zr	Nb	Cs	Ba	V	Co	Cu	Zn
205-1253A-*													
1R-2, 31-33	373	4.87	9.55	1318	6.80	10.80	4.57	0.26	2377	42.9	17.41	360	102
2R-2, 28-30	378	9.44	17.62	1314	17.72	45.65	10.62	0.39	3345	40.1	13.01	226	127
3R-2, 3-5	387	7.76	10.59	1120	13.43	31.25	8.59	0.21	2718	43.5	14.56	86	159
3R-2, 92-94	388	4.06	3.48	173	11.97	45.63	8.05	0.10	1232	32.8	6.15	8	51
3R-3, 13-16	388.5	13.44	11.75	760	14.14	32.98	10.72	0.24	2503	93.1	19.36	177	132
3R-3, 77-79	389	7.41	7.48	733	17.00	55.08	11.70	0.25	3215	64.5	10.43	144	130
4R-1, 15-16	395	11.17	6.97	778	12.30	30.86	4.63	0.22	2523	62.2	13.60	190	91
4R-1, 37-39	395.5	11.94	5.35	410	7.82	25.67	3.37	0.16	1100	ND	ND	ND	ND
4R-1, 43-44	395.6	5.26	4.47	718	12.05	23.19	3.47	0.18	3186	26.0	4.32	110	84
4R-1, 66-67	396.7	ND	ND	ND	ND	ND	ND	ND	ND	ND	ND	ND	ND
4R-1, 79-81	396.8	12.59	1.24	378	10.88	30.87	4.62	0.04	709	77.6	11.93	4	111
4R-3, 79-80	399	8.06	2.86	251	9.13	29.09	3.86	0.06	222	59.5	7.16	7	29
4R-4, 44-46	399.7	4.25	7.03	885	7.87	11.61	2.57	0.18	1145	24.4	4.29	47	48
5R-1, 0-5	400	7.98	7.62	173	13.10	19.65	2.23	0.36	481	ND	ND	ND	ND
205-1253A-†													
10R-2, 49-51	431.00	5.30	1.18	679	17.35	33.27	4.61	0.01	663	31.8	5.35	46	35
10R-2, 59-73	431.20	8.34	2.85	752	22.47	51.29	6.64	0.05	3382	69.8	18.19	192	113
10R-2, 96-78	431.50	11.16	7.14	735	17.87	43.31	5.26	0.11	2075	74.1	10.96	103	80
10R-2, 116-118	431.70	7.18	6.09	963	15.14	33.09	4.49	0.19	2401	47.2	7.22	102	80
10R-2, 123-124	431.80	9.20	9.54	828	24.86	50.43	6.66	0.28	4143	76.0	9.61	319	150
11R-1, 7-9	436.10	4.86	1.63	730	10.05	15.06	1.44	0.04	1490	39.6	5.21	68	64
11R-1, 19-21	436.20	6.34	1.49	821	13.63	22.24	2.74	0.04	1688	58.6	7.56	73	95
11R-1, 38-40	436.40	3.16	2.82	912	10.22	14.15	1.58	0.08	1748	27.5	3.24	155	70
11R-1, 81-96	436.80	5.14	1.88	1008	16.28	28.03	3.82	0.08	2189	49.7	5.70	86	91
11R-2, 2-4	437.00	13.27	4.54	599	11.56	31.56	3.16	0.12	1188	118.8	18.50	106	91
11R-2, 14-16	437.10	9.11	1.67	847	14.86	32.82	3.76	0.04	2769	91.1	13.04	128	111
11R-2, 34-35	437.50	10.74	2.64	828	20.83	45.75	6.48	0.11	3741	91.5	11.72	119	132
11R-2, 54-56	437.70	4.83	3.93	817	13.05	32.58	4.11	0.14	2568	36.9	6.25	52	77

Table T2. Measured and reference values for rock standards JB-2 and JB-1A.

	JB-2			JB1-A		
	Certified value	Measured value	Accuracy (%)	Certified value	Measured value	Accuracy (%)
Sc	54	55	1.55	29	30	2.80
Rb	6.2	6	2.40	41	41	0.05
Sr	178	166	7.30	443	459	3.53
Y	26	24	8.27	25	24	2.42
Zr	52	55	4.71	144	145	0.47
Nb	0.6	1	6.90	27	27	0.04
Cs	0.9	1	2.43	1.2	1	19.31
V	575	567	1.35	205	206	0.51
Co	38	39	1.64	38.6	38	1.74
Cu	225	226	0.45	56.7	52	8.67
Zn	108	115	5.96	82.1	71	16.14
Ba	208	204	1.92	497	499	0.33
		Average:	3.74		Average:	4.67